Received: 16 May 2020 | Revised: 30 September 2020 | Accepted: 1 October 2020

DOI: 10.1002/jbio.202000191

JOURNAL OF BIOPHOTONICS

LETTER

Non-local means improves total-variation constrained photoacoustic image reconstruction

Phaneendra K. Yalavarthy[1] | **Sandeep Kumar Kalva**[2] | **Manojit Pramanik**[2] | **Jaya Prakash**[3*]

[1]Department of Computational and Data Sciences, Indian Institute of Science, Bangalore, India

[2]School of Chemical and Biomedical Engineering, Nanyang Technological University, Singapore

[3]Department of Instrumentation and Applied Physics, Indian Institute of Science, Bangalore, India

***Correspondence**
Jaya Prakash, Department of Instrumentation and Applied Physics, Indian Institute of Science, Bangalore India 560012.
Email: jayap@iisc.ac.in

Funding information
Department of Biotechnology, Ministry of Science and Technology, Grant/Award Number: IYBA; Infosys Foundation, Infosys Young Investigator Award, Grant/Award Number: IYBA; Department of Science and Technology, India, Grant/Award Number: ICPS cluster funding (T-851); IFTAS-CDS; Indian Institute of Science, Grant/Award Number: Startup Grant

Abstract

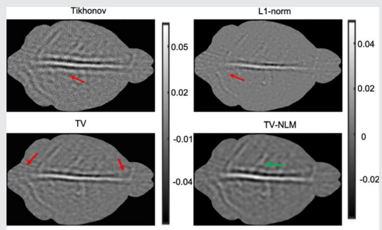

Photoacoustic/Optoacoustic tomography aims to reconstruct maps of the initial pressure rise induced by the absorption of light pulses in tissue. This reconstruction is an ill-conditioned and under-determined problem, when the data acquisition protocol involves limited detection positions. The aim of the work is to develop an inversion method which integrates denoising procedure within the iterative model-based reconstruction to improve quantitative performance of optoacoustic imaging. Among the model-based schemes, total-variation (TV) constrained reconstruction scheme is a popular approach. In this work, a two-step approach was proposed for improving the TV constrained optoacoustic inversion by adding a non-local means based filtering step within each TV iteration. Compared to TV-based reconstruction, inclusion of this non-local means step resulted in signal-to-noise ratio improvement of 2.5 dB in the reconstructed optoacoustic images.

KEYWORDS
deconvolution, image reconstruction, inverse problems, photoacoustic tomography, regularization theory

1. | INTRODUCTION

Photoacoustic tomography (PAT)/Optoacoustic tomography (OAT) has been widely used to image intrinsic and extrinsic chromophores at very high spatio-temporal resolution.[1] PAT/OAT problem involves utilizing the recorded acoustic measurements to estimate the initial pressure rise inside the tissue. The estimation of the initial pressure rise can be performed by inverting the wave equation either using analytical schemes or model-based schemes.[2,3] Analytical type methods are attractive due to their low computational complexity.[4] However analytical formulation for irregular imaging geometries (which is often the case) is not straight forward.[5] Moreover, model-based methods have demonstrated potential in providing reconstructions with higher quantitative accuracy compared to analytical methods with noisy and limited data.[2,3] Model-based reconstruction involves matching the measured acoustic signal with the signals predicted by the model, in this work, the model was generated by using impulse response approach.[3] Model-based methods have been studied extensively in the literature, Rosenthal et al. proposed a interpolated matrix model inversion scheme wherein the solution of the forward model was discretized using interpolation functions.[6] The developed model was exhaustively studied along with non-negativity constraints (as absorption coefficient should not take negative values).[7,8] Physics-based transducer modeling was also taken up, wherein the spatial impulse response and electrical impulse response was modeled and deconvolved to improve optoacoustic image quality.[9,10] Methods have also been developed for jointly reconstructing the initial pressure rise and speed of sound using optoacoustic measurements.[11] More recently Bayesian approaches were developed for uncertainty quantification while performing three-dimensional optoacoustic inversion.[12]

Minimizing the residue does not generate accurate image representation in limited data scenarios due to the ill-conditioned/under-determined nature of the problem. Hence, additional constraint in the form of prior statistics about the image have been applied as a regularization term during the inversion.[3,13] Different forms of constraints including Tikhonov regularization, sparse regularization, total-variation, and non-quadratic type regularization[6–8,13,14] were applied earlier. Tikhonov regularization is a traditional approach, wherein the emphasis is to reconstruct images that are smooth and suppress noise, thereby reducing sharp features in the reconstructed images. Sparsity and total-variation (TV) constrained reconstructions were also deployed to reconstruct sharp features.

The TV-regularization based image reconstruction is a non-smooth type inversion scheme and requires an iterative process to converge to a minima. The TV regularization is known to generate accurate image representation, but generates noisy images especially in cases where the data noise level is high. More importantly, the choice of regularization parameter plays a critical role in generating accurate optoacoustic images. Specifically the value of regularization parameter is heavily dependent on the level of noise present in the data. In this work, we incorporated the non-local means (NLM) based denoising[15] algorithm within each iteration of the TV inversion. NLM was expected to identify similar patches (having similar noise statistics) in optoacoustic images, and then average across these patches to denoise the reconstructed image at every iteration.[15] This work aims to show that the incorporation of NLM filtering will reduce the bias towards the choice of regularization, and improve reconstruction performance with noisy data.

2. | MATERIALS AND METHODS

The forward model in PAT/OAT can be written as,[3]

$$\mathbf{A}x = b \tag{1}$$

where the dimension of the matrix **A** is 30,720 × 40,401 (image size being 201 × 201) and is computed using an impulse response approach, wherein impulse response of every pixel in the imaging domain was used to build the matrix as explained in Reference [3]. The impulse response was calculated using the k-Wave toolbox.[16] Model-based image reconstruction using TV regularization exploits the fact that edges are sparse in nature. TV minimization cost function can be written as,

$$x_{TV} = arg \quad min_x \left(\|Ax - b\|_2^2 + \lambda |x|_{TV} \right) \tag{2}$$

where $|x|_{TV}$ is the anisotropic total variation term given as $|x|_{TV} = \sum_i | x_i - x_{i-1}|$, λ is the regularization parameter, and the L_2-norm distance is given as $\|x\|_2^2 = \left(x_1^2 + x_2^2 + \dots + x_n^2\right)$ with x being a $n \times 1$ vector. Equation 2 was minimized using an iterative reweighted least square (IRLS) scheme,[17] wherein the derivative is,

$$\frac{\partial x_{TV}}{\partial x} = \left(A^T A + \lambda W\right)^{-1} A^T b \tag{3}$$

where the TV weighting term (W) can be written as,

$$W = diag\left(\frac{1}{max\left(\sum_j \left(|x_j - x_{j-1}|\right), th \right)} \right) \tag{4}$$

here th represents the threshold, which was set to 0.01 and |. | represents absolute value. The IRLS algorithm for minimizing Equation 2 was ran for 10 iterations, as the change in the residual was observed to be in the order of 10^{-4}.

Since TV based scheme performance is suboptimal in noisy environments and being sensitive to the choice of regularization (data-dependent), this work included an additional denoising step within the IRLS framework to address these shortcomings. The proposed method utilizes NLM based denoising step within the IRLS framework. The NLM based method has been used extensively in areas of image processing and medical imaging.[15,18] However in these works, NLM was used as a post-processing step after the image reconstruction procedure. In contrary, the presented work involved integrating the NLM denoising step within each IRLS iteration of TV minimization. The main strength of NLM denoising over local filters (based on spatial kernels) or frequency domain filters is to systematically search for all possible denoised outcomes that the image can provide.[15] In other words, while performing NLM denoising at a pixel location i in the image x, the NLM method assigns a mean value of all pixel location whose Gaussian neighborhood looks like neighborhood of x_i. Degree of filtering in the NLM algorithm plays a crucial role while perform the denoising.[15] The details of TV-NLM algorithm is

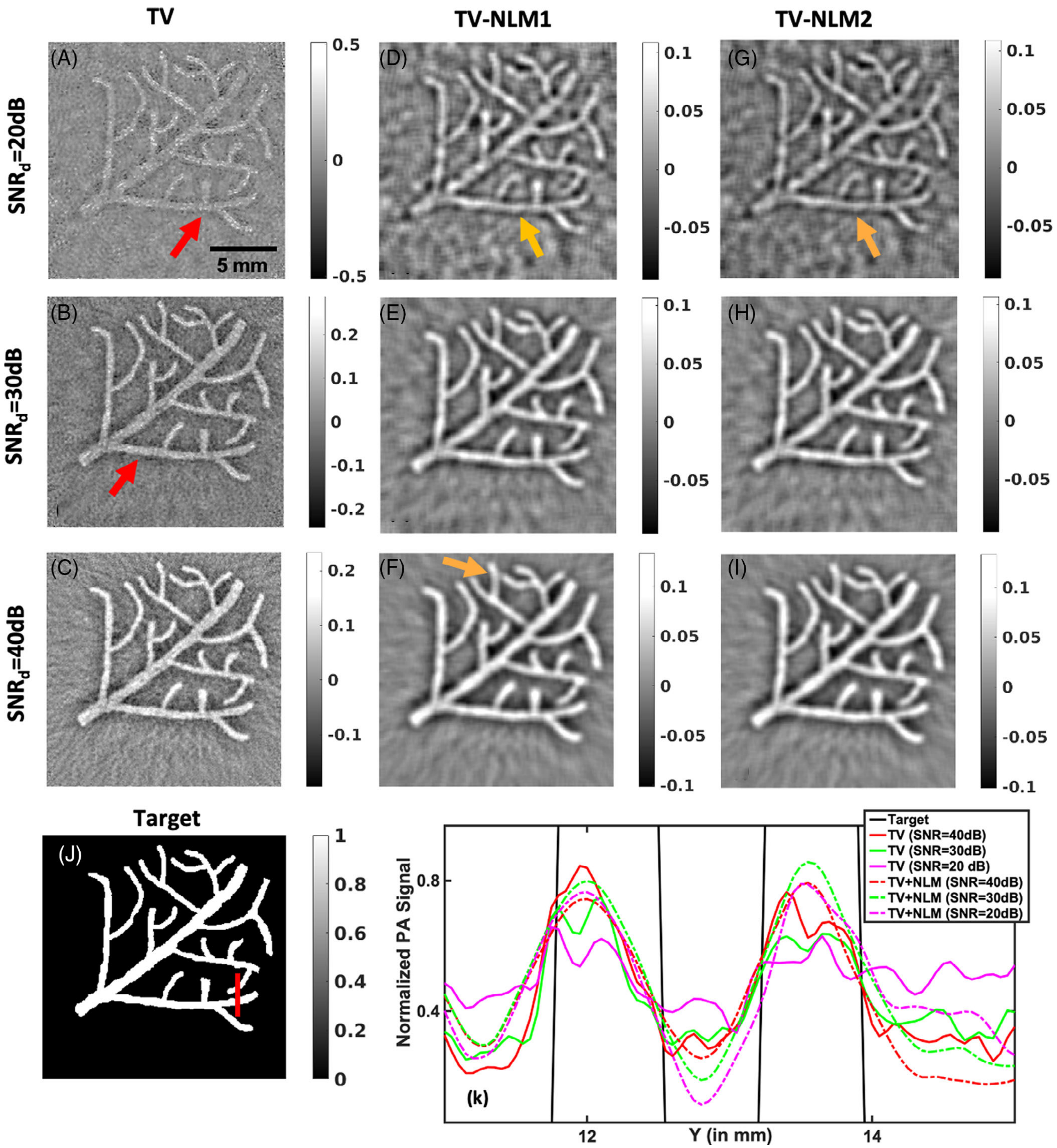

FIGURE 1 Comparison of the performance of TV, proposed TV-NLM method using blood vessel phantom: Images reconstructed with TV regularization scheme for, A, 20 dB; B, 30 dB; C, 40 dB SNR of data. Reconstructions using TV-NLM1 (degree of filtering was set to 2) reconstruction scheme for, D, 20 dB; E, 30 dB; F, 40 dB SNR of data. Reconstructions pertaining to TV-NLM2 (degree of filtering was set to 3) scheme for, G, 20 dB; H, 30 dB; I, 40 dB SNR of data. Original blood vessel phantom is shown in J. Line plots for the results pertaining to, A-I,) across the red line show in, J, is indicated in, K

provided as Algorithm-1 in the supplementary. In the TV-NLM approach, two regularization constraints were applied while performing the reconstruction (one in the form of TV, and the other in the form of NLM). Note that the IRLS-based TV implementation (minimizing Equation 2) is similar to Algorithm-1 without the NLM step (step-4 in Algorithm-1 shown in the supplementary). The computational complexity of TV and TV-NLM approach is $O(k^3 \times N^2)$ and $O(N^2 \times k^3 \times N^2)$, respectively, here k represents bidiagonalization iterations and N^2 is the total number of pixels. As with any two-step reconstruction algorithm, the computational complexity of the proposed TV-NLM approach is higher than the TV alone. The TV approach took 2132 seconds and TV-NLM scheme took 2918 seconds. This increase in computational complexity is worth as it results in improved reconstruction results. Among the NLM and TV reconstruction parameters, the choice of regularization parameter and degree of filtering depends on the noise level in the data, therefore this work studied the effect of these parameters with varying data noise levels. Typically, the degree of filtering value should be set to higher values when the received data is highly noisy. In low noise case, the degree of filtering must be set to lower values. We have also performed Tikhonov and L1-norm-based reconstructions as explained in Reference [14]. The reconstruction performance from different algorithms were compared using standard figure of merits, like Pearson correlation (PC, computed on 1D vectorized image), contrast to noise ratio (CNR), structural similarity (SSIM) between ground truth and reconstructed images, and signal to noise ratio (SNR) in the reconstructed image,[14] the definition of these metrics are given in the supplementary.

Numerical blood vessel phantom with initial pressure rise of 1 kPa was considered for comparing the quantitative accuracy of TV and proposed TV-NLM based reconstruction. Experimental data from in-vivo rat brain was also used to compare the performance of different reconstruction methods explained here. The details about the experimental setup and the data collection strategy from in-vivo rat brain can be found in Reference [19]. The collected experimental OA data were pre-processed with a bandpass filter having a bandwidth of 0.1–8 MHz.

Numerically simulated data was generated on a fine grid having a size of 50.1×50.1mm (discretized to 1002×1002) pixels, with the imaging region containing the blood vessel phantom being restricted to 20.1×20.1mm, corresponding to 402×402 pixels. The blood vessel phantom in 402×402 pixels generated a optoacoustic wave, which was propagated using kWave toolbox.[16] In order to avoid inverse crime, this numerical data was utilized in the inversion process to reconstruct a domain of 201×201 pixel. Simulated data was sampled at sixty detector positions, with the detector characteristics of 70% bandwidth and a center frequency of 2.25 MHz. The detector positions were sampled equidistantly on a circle having a radius of 22 mm. The in-silico time-series data was sampled at 50 ns (simulating DAQ sampling), with total time samples being 512. For numerical simulations, the medium was assumed to have uniform speed of sound of 1500 m/s. Lastly the numerical data acquired at sixty detector positions was added with additive white Gaussian noise (AWGN) resulting in different SNR levels of data (20 dB, 30 dB and 40 dB). In the case of experimental data (rat brain data), a system matrix with a dimension of $51{,}200 \times 40{,}000$

TABLE 1 Comparison of quantitative performance (using SSIM, PC, and CNR) with TV, and proposed TV-NLM method for different values of regularization parameter (λ) and SNR_d = 30dB and 40 dB cases (reconstructed images are shown in Figure 2)

SNR_d/λ	**λ = 0.00001**		**λ = 0.0001**		**λ = 0.001**	
SNR_d	TV	PC = 0.65	TV	**PC = 0.66**	TV	PC = 0.54
=30 dB		CNR = 2.43		**CNR = 2.57**		CNR = 2.12
		SSIM = 0.1438		SSIM = 0.2003		**SSIM = 0.3366**
	TV-NLM	PC = 0.70	TV-NLM	**PC = 0.71**	TV-NLM	PC = 0.63
		CNR = 2.79		**CNR = 2.88**		CNR = 2.35
		SSIM = 0.3225		SSIM = 0.3829		**SSIM = 0.4972**
SNR_d	TV	**PC = 0.72**	TV	PC = 0.62	TV	PC = 0.57
=40 dB		**CNR = 3.08**		CNR = 2.56		CNR = 2.25
		SSIM = 0.2444		SSIM = 0.3438		**SSIM = 0.3715**
	TV-NLM	**PC = 0.74**	TV-NLM	PC = 0.69	TV-NLM	PC = 0.66
		CNR = 3.11		CNR = 2.73		CNR = 2.47
		SSIM = 0.4017		SSIM = 0.4937		**SSIM = 0.5168**

(corresponding to 51,200: 512 time samples for 100 detector positions and 40,000: 200 × 200 reconstruction grid) was built.

3. | RESULTS AND DISCUSSION

Initially, TV-NLM method was compared to stand-alone TV by varying the amount of noise in the simulated data. The reconstruction results using different algorithms pertaining to blood vessel phantom (Figure 1J) were provided in Figure 1. Figure 1A shows the reconstruction result using TV regularization approach for data SNR (SNR_d) of 20 dB. The red arrow in Figure 1A indicates regions where streak type pattern starts appearing, resulting in shadowing of blood vessel signal (with lesser contrast). However, reconstruction results pertaining to TV-NLM method (shown in Figures 1D,G) reconstructs

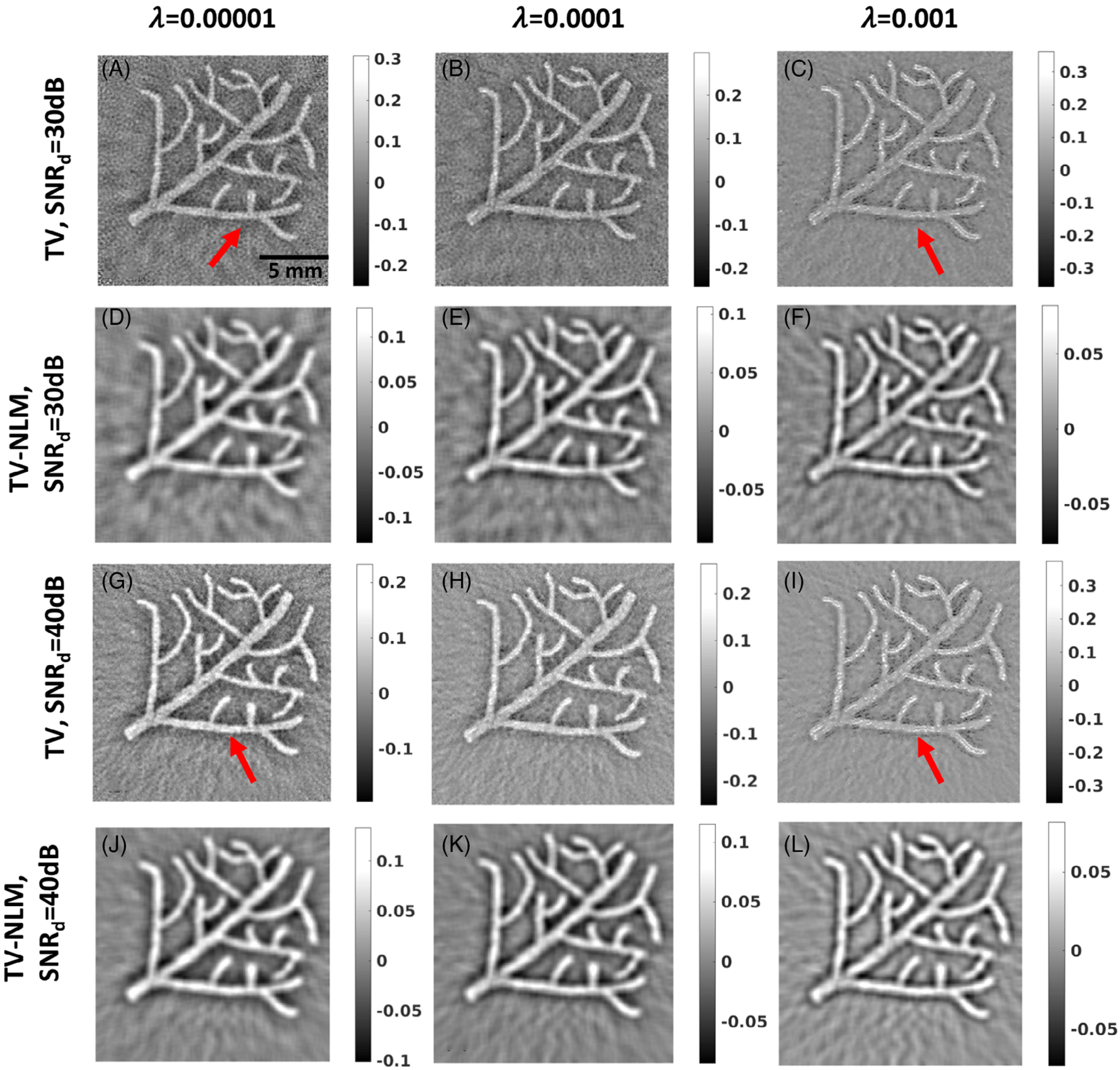

FIGURE 2 Analysis of the effect of regularization on TV based image reconstruction: A-C, Reconstructed image with TV regularization scheme for SNR_d = 30dB and λ = 0.00001, 0.0001, and 0.001. D-F, Reconstructed image with proposed TV-NLM regularization scheme for SNR_d = 30dB and λ = 0.00001, 0.0001, and 0.001. G-I, Reconstructed image with TV regularization scheme for SNR_d = 40dB and λ = 0.00001, 0.0001, and 0.001. J-L Reconstructed image with proposed TV-NLM regularization scheme for SNR_d = 40dB and λ = 0.00001, 0.0001, and 0.001

vasculature with improved contrast (as indicated by orange arrows). Note that the degree of filtering (i.e. *fil* in Algorithm-1 in the supplementary) was set to 2 in case of TV-NLM1 and 3 in case of TV-NLM2. Figure 1B indicates the reconstruction output with TV reconstruction scheme with SNR_d = 30dB. Similar to the 20 dB case, TV-NLM approach was able to generate more accurate representation of blood vasculature with greater contrast and reduced streak artifacts (see Figures 1(E) & (H)). Lastly, the TV-based image reconstruction result with SNR_d = 40dB was shown in Figure 1C, which showed similar trend. As expected, inclusion of NLM step within the TV iteration blurred the image (as shown by yellow arrow in Figure 1F), nevertheless reducing the noise in the reconstructed images (see Figures 1F,I). NLM algorithm involves finding similar patches and systematically searching for all desired denoised outcomes. In this process, it is expected to provided smooth (blurry) image with reduced noise (denoising algorithm will typically reduce high frequency context resulting in blurry solution); which can be seen in Figure 1F,I as compared to Figure 1C. Note that in these results, optimal reconstruction parameters were chosen automatically to result in maximum PC and CNR values. Automatically choosing the reconstruction parameter is important to avoid biasing the reconstruction results while comparing different algorithms, and further this would allow biologists to perform unbiased analysis. Since different constraints are being applied with algorithms used in this work, the estimated optimal reconstruction parameter value is not expected to be similar, the resulted optimal reconstruction parameter values were tabulated in the Supplementary. Lastly, Figure 1K shows the comparison of line plot along the red line of Figure 1J for the results presented in Figures 1A-I. From the line plot, one can infer that the TV-NLM approach (blue, green and yellow lines) provides accurate image representation in high-noise environment and is able to improve reconstruction results provided by stand-alone TV approach (red, cyan and pink lines) in low-noise environment. Figure 1 indicates that TV-NLM scheme is stable for varying degree of filtering in the NLM step.

The choice of regularization plays a crucial role in limited data optoacoustic image reconstruction, and is heavily influenced by the amount of noise in the data. Hence, the next set of simulations were performed to assess whether the proposed TV-NLM approach is less susceptible to the choice of regularization parameter. Figures 2A-C correspond to reconstruction performance of TV based scheme with SNR_d = 30dB and $\lambda = 0.00001$, 0.0001, and 0.001, respectively. Figures 2D-F show the reconstruction results using proposed TV-NLM (with *fil* = 2) based scheme with SNR_d = 30dB and λ = 0.00001, 0.0001, and 0.001, respectively. From Figures 2A-F, it is obvious that TV based reconstruction is heavily biased by the choice of regularization,

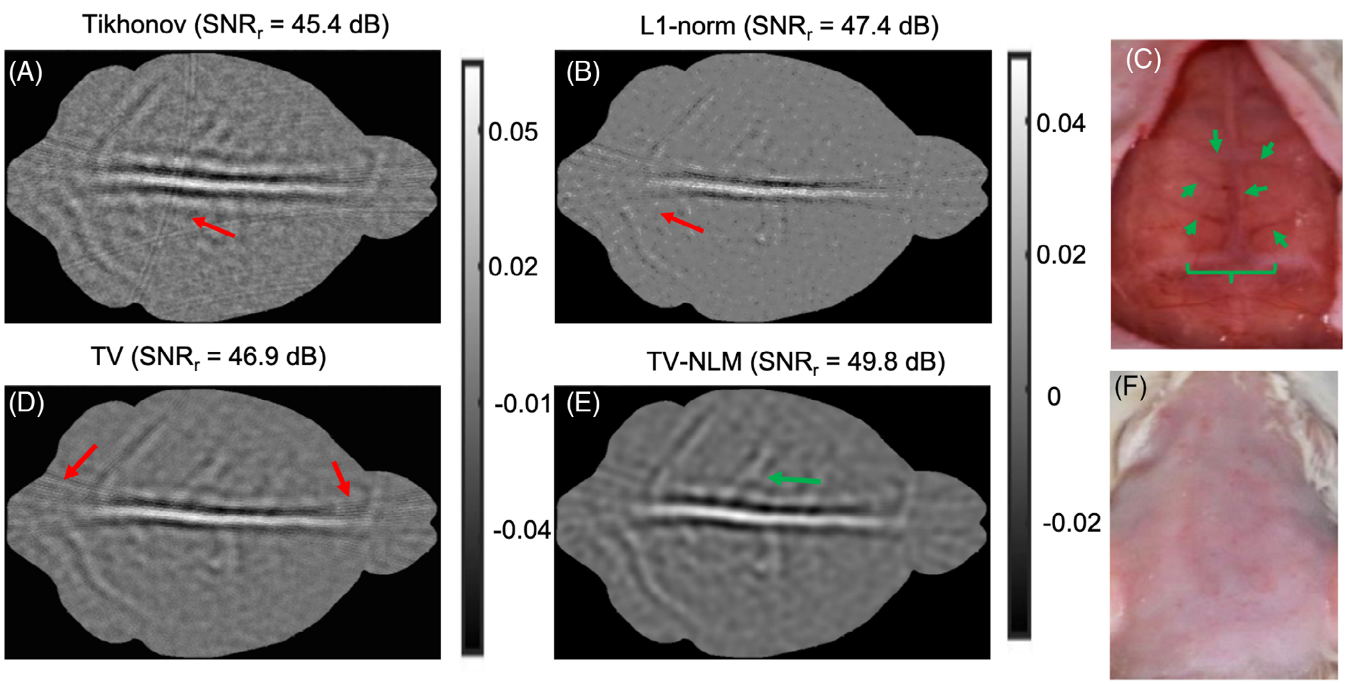

FIGURE 3 Reconstructed results pertaining to in-vivo rat brain imaging using, A, Tikhonov regularization, B, L1-norm regularization. C, Open-skull image. Reconstructed results pertaining to, D, TV regularization, E, proposed TV-NLM (with degree of filter = 3). F, shaved rat brain for acquisition

i.e. higher value of regularization seems to amplify noise (shown by red arrow in Figure 2C). In contrary, TV-NLM scheme is able to generate similar reconstructions when λ is varying from 0.00001 to 0.001. Figures 2G-I corresponds to reconstruction results using TV-based scheme with SNR_d = 40dB and $\lambda = 0.00001$, 0.0001, and 0.001, respectively. Figures 2J-L indicates the reconstruction outputs using proposed TV-NLM (with $fil = 2$) based scheme with SNR_d = 40dB and $\lambda = 0.00001$, 0.0001, and 0.001, respectively. The reconstruction results show similar trend as observed in the case of SNR_d = 30dB. Further, Table 1 reports the quantitative comparison of the proposed TV-NLM (degree of filtering being 2) scheme with TV-based approach using quantitative metric like SSIM, PC and CNR. Overall, TV-NLM scheme seems to outperform TV approach with varying noise levels in the simulated data and for different choice of λ.

Lastly, the performance of Tikhonov, L1-norm, TV, and TV-NLM schemes were assessed by imaging in-vivo rat brain (OA data were collected on Figure 3F and Figure 3C is open-skull image for comparison). Note that the obtained in-vivo reconstruction results were cropped to denote only the brain region of the image for better visualization using ImageJ. Figure 3A corresponds to the reconstruction result using Tikhonov-based scheme, note aberration artifacts seems to appear in the reconstruction result as indicated by red arrows in Figure 3A. Figure 3B corresponds to the reconstruction result using L1-norm regularization, which has streak type artifacts. Figure 3D shows the reconstruction result corresponding to TV regularization, which seems to have generated streak type artifacts at the boundaries of the cropped brain images as indicated by red arrow. Figure 3E shows the TV-NLM reconstruction with degree of filtering being 3. As shown by red arrow in Figure 3A,B,D and green arrow in Figures 3E, inclusion of NLM step within the TV iteration reconstructs the vasculature in the brain more accurately devoid of reconstruction artifacts, the same is reflected in the computed SNR values shown above each figure. Note that in the experimental case, reconstruction parameters were chosen automatically to result in maximum SNR with TV and TV + NLM schemes. The performance of different reconstruction methods using another set of experimental data (using horse-hair phantom) is shown in the supplementary.

Previous works have utilized patch-based processing (in the form of Block Matching 3D [BM3D]) for sparse view optoacoustic tomography in combination with Fourier domain-based analytical reconstruction.[20] The BM3D-based method was found to provide reconstruction which are superior compared to universal backprojection algorithm, however the analysis was restricted to phantoms and ex-vivo samples. In here, a two-step framework was proposed by including the NLM-based image-domain processing within the model-based reconstruction framework. This work was limited to integrating NLM with TV-based objective function, however, the same can be extended to other constraints like fractional regularization, sparsity regularization, and non-quadratic potential functions.[13, 14]

4. | CONCLUSIONS

In summary, a simple and well established post-processing filter (NLM) was included in the total-variation constrained optoacoustic image reconstruction within each iteration. The results indicate that the proposed TV-NLM method outperforms than TV reconstruction in high-noise environments. Importantly, this work established that the TV-NLM scheme was able to generate similar reconstruction results for a wide range of regularization parameter choice, that is, $\lambda = 0.00001$ to 0.001 with varying data noise levels. Lastly, quantitative metrics revealed that TV-NLM scheme was able to generate reconstructions that had atleast 10% more contrast compared to traditional TV reconstruction.

ACKNOWLEDGMENTS

Phaneendra K. Yalavarthy acknowledges the DST-ICPS cluster funding (T-851) for the data science program. Part of the work is supported through IFTAS-CDS Collaborative Laboratory of Data Science and Engineering. Jaya Prakash acknowledges the IISc Startup Grant, Infosys Young Investigator Award, as well as DBT-IYBA Program.

CONFLICT OF INTERESTS

The authors declare that there are no conflicts of interest related to this article.

DATA AVAILABILITY STATEMENT

The in-silico data that support the findings of this study are available from the corresponding author upon reasonable request.

ORCID

Phaneendra K. Yalavarthy https://orcid.org/0000-0003-4810-352X

Manojit Pramanik https://orcid.org/0000-0003-2865-5714

Jaya Prakash https://orcid.org/0000-0002-2375-154X

REFERENCES

[1] V. Ntziachristos, *Nat. Methods* **2010**, *7*(8), 603.
[2] A. Rosenthal, V. Ntziachristos, D. Razansky, *Curr. Med. Img. Rev.* **2013**, *9*, 318.
[3] J. Prakash, A. S. Raju, C. Shaw, M. Pramanik, P. K. Yalavarthy, *Biomed. Opt. Exp.* **2014**, *5*, 1363.
[4] M. Xu, L. V. Wang, *Phys. Rev. E* **2005**, *71*(1), 016706.
[5] P. Burgholzer, G. J. Matt, M. Haltmeier, G. Paultauf, *Phy. Rev. E* **2007**, *74*(5), 046706.
[6] A. Rosenthal, D. Razansky, V. Ntziachristos, *IEEE Trans. Med. Img.* **2010**, *29*(6), 1275.
[7] L. Ding, X. L. Dean-Ben, C. Lutzweiler, D. Razansky, V. Ntziachristos, *Phys. Med. Biol.* **2015**, *60*, 6733.
[8] J. Prakash, S. Mandal, D. Razansky, V. Ntziachristos, *Biomed. Img.* **2019**, *66*(9), 2604.
[9] M. A. A. Caballero, J. Gateau, X. L. Daan-Ben, V. Ntziachristos, *Med. Img.* **2013**, *33*(2), 433.
[10] K. B. Chowdhury, J. Prakash, A. Karlas, D. Justel, V. Ntziachristos, *IEEE Trans. Med. Img* **2020**, *39*(10), 3218.
[11] T. P. Matthews, J. Poudel, L. Lei, L. V. Wang, M. A. Anastasio, *SIAM J. Img., Sci.* **2018**, *11*(2), 1560.
[12] J. Tick, *J. Acoustical Soc. America* **2018**, *144*(4), 2061.
[13] Y. Han, L. Ding, X. L. Dean-Ben, D. Razansky, J. Prakash, V. Ntziachristos, *Opt. Lett.* **2017**, *42*(5), 979.
[14] J. Prakash, D. Sanny, S. K. Kalva, M. Pramanik, P. K. Yalavarthy, *IEEE Trans. Med. Img.* **2019**, *38*(8), 1935.
[15] A. Baudes, B. Coll, *J. Morel in: IEEE Conf. on Comp. Vision and Pattern Recognition* **2005**, 8624018.
[16] B. E. Treeby, B. T. Cox, *J. Biomed. Opt.* **2010**, *15*, 021314.
[17] E. Candes, M. B. Wakin, S. P. Boyd, *J. Fourier Anal. Appl.* **2008**, *14*, 877.
[18] J. Dutta, R. M. Leahy, Q. Li, *PLoS One* **2013**, *8*(12), e81390.
[19] S. Gutta, S. K. Kalva, M. Pramanik, P. K. Yalavarthy, *Med. Phy.* **2018**, *45*(8), 3749.
[20] Y. Wang, T. Lu, J. Li, W. Wan, W. Ma, L. Zhang, Z. Zhou, J. Jiang, H. Zhao, F. Gao, *Biomed. Opt. Exp.* **2018**, *9*(9), 4569.

SUPPORTING INFORMATION

Additional supporting information may be found online in the Supporting Information section at the end of this article.

How to cite this article: Yalavarthy PK, Kalva SK, Pramanik M, Prakash J. Non-local means improves total-variation constrained photoacoustic image reconstruction. *J. Biophotonics*. 2021;14:e202000191. https://doi.org/10.1002/jbio.202000191